Cognitive Neurodynamics (2019) 13:201–217
https://doi.org/10.1007/s11571-018-9514-0

RESEARCH ARTICLE

The beta oscillation conditions in a simplified basal ganglia network

Bing Hu[1,2] · Xiyezi Diao[3] · Heng Guo[3] · Shasha Deng[3] · Yu Shi[3] · Yuqi Deng[3] · Liqing Zong[3]

Received: 15 April 2018 / Revised: 20 November 2018 / Accepted: 27 November 2018 / Published online: 4 December 2018
© Springer Nature B.V. 2018

Abstract

Parkinson's disease is a type of motor dysfunction disease that is induced mainly by abnormal interactions between the subthalamic nucleus (STN) and globus pallidus (GP) neurons. Periodic oscillatory activities with frequencies of 13–30 Hz are the main physiological characteristics of Parkinson's disease. In this paper, we built a class of STN–GP networks to explore beta oscillation conditions. A theoretical formula was obtained for generating oscillations without internal GP connections. Based on this formula, we studied the effects of cortex inputs, striatum inputs, coupling weights and delays on oscillation conditions, and the theoretical results are in good agreement with the numerical results. The onset mechanism can be explained by the model, and the internal GP connection has little effect on oscillations. Finally, we compared oscillation conditions with those in previous studies and found that the delays and coupling weights required for generating oscillations may decrease as the number of nuclei increases. We hope that the results obtained will inspire future theoretical and experimental studies.

Keywords Parkinson's disease · Globus pallidus · Subthalamic nucleus · Beta oscillation conditions

Introduction

Parkinson's disease (PD) is a type of neurodegenerative disease that is mainly associated with motor dysfunction, such as static tremor, rigidity, bradykinesia, and festinating gait (Moustafa et al. 2016; Yi et al. 2017). The death of dopaminergic neurons in the mid-brain substantia nigra pars compacta is the main pathogenies (Jankovic 2008). Many studies have established that exaggerated synchronous oscillatory activities in the basal ganglia, especially in the subthalamic nuclei (STN) and globus pallidus nuclei (GP), are the main pathological features of PD patients (Levy et al. 2000; Brown et al. 2001; Ahn et al. 2015). Due to different clinical manifestations, the frequency of oscillations is also different, including typical beta oscillations (13–30 Hz) (Little and Brown 2014; Cole et al. 2017) and typical static tremors (4–6 Hz) (Camara et al. 2015; Malekmohammadi et al. 2016), and so on. The earliest papers showed that PD was associated with increased oscillatory and synchrony discharges within the basal ganglia, information that emerged from studies of the 1-methyl-4-phenyl-1,2,3,6-tetrahydropyridine (MPTP) primate model (Bergman et al. 1994). Thus, there are an increasing number of research results to support these perspectives, especially the computational models (Gillies et al. 2002; Terman et al. 2002; Rubin and Terman 2004; Humphries et al. 2006; Leblois et al. 2006; Kumar et al. 2011; Muralidharan et al. 2013). For example, Rubin and Terman (2004) found that high-frequency current stimulation of the STN can inhibit pathological thalamic oscillatory rhythmicity in a simplified basal ganglia-thalamus computational model by increasing the firing rates of the action target. Kumar et al. (2011) noted that the strength of inhibitory inputs from the striatum to the globus pallidus external (GPe) is a key factor for generating and controlling oscillations in the basal ganglia, which provided a unified framework to explain the healthy state, the dopamine-depleted state and the quenching of oscillations under

✉ Bing Hu
djhubingst@163.com

[1] Department of Applied Mathematics, Zhejiang University of Technology, Hangzhou 310023, China

[2] Key Laboratory of Systems Biology, Innovation Center for Cell Signaling Network, Institute of Biochemistry and Cell Biology, Shanghai Institute of Biological Sciences, Chinese Academy of Sciences, Shanghai 200031, China

[3] Department of Mathematics and Statistics, College of Science, Huazhong Agricultural University, Wuhan 430070, China

deep brain stimulation in the basal ganglia. Holt and Netoff (2014) employed a physiologically realistic basal ganglia network computational model to investigate the onset of a 34 Hz oscillation in the Parkinson state. Shouno et al. (2017) found, by using a spiking neuron model of the STN–GPe circuit, that the recurrent circuit between the STN and GPe involved in generating and maintaining parkinsonian oscillations and cortical excitatory input to the STN can amplify or suppress pathological oscillations. The beta oscillations that appeared in the basal ganglia mean field model were first observed by van Albada et al. (2009) and van Albada and Robinson (2009); however, the oscillation activities of these models originated from the corticothalamic networks. The first mean firing-rate model that showed beta oscillations directly originating from the STN–GPe network was developed by Holgado et al. (2010) and is a simplified basal ganglia computational model formed by one STN population and one GPe population, where the approximate theoretical oscillation conditions were obtained by the quasilinearization method. Pavlides et al. (2012) employed the same model to obtain an improved condition for oscillation by using the Laplace transformation, and they found that the theoretical results compared very well with the numerical results. At about the same time, beta oscillations were obtained in STN–GPe networks in a much more realistic ion channels kinetics model, which are quantitatively similar to actual experimental data from human subjects with Parkinson's disease (Park et al. 2011). Recently, Pavlides et al. (2015) explored possible mechanisms for the generation of excessive beta oscillations of Parkinson's disease in a simplified basal ganglia-corticothalamic computational model.

In addition to the STN and GP, the basal ganglia also contain many other types of neurons, such as the striatum, which mainly projects inhibitory outputs to the GP and plays a key role in generating and controlling oscillations (Belluscio et al. 2014; Surmeier et al. 2014; Alcacer et al. 2017). In addition to the internal links, the firing activities of the basal ganglia are also greatly affected by the outputs from other organizations, such as the thalamocortical system. From the perspective of anatomical structure, the cortex is the main excitatory input source to the STN. Therefore, the striatum and cortex may both exert great effects on oscillations, the mechanisms of which are currently receiving little consideration. Moreover, some critical factors in the model, such as the coupling strengths between the STN and GP, the time required for signal transmissions on a specific pathway, etc., also have great effects on oscillations, and the relevant mechanisms are still unclear. Related methods recently employed in exploring synchronization theory (Jiancheng et al. 2017; Kim and Lim 2016, 2018; Wang et al. 2018), brain connections and dynamic behaviours (Dasdemir et al. 2017; Hu et al. 2018) may also be suitable for studying Parkinson's disease in the future.

Inspired by the above theoretical research progress, we built an improved basal ganglia model, which contains two STN populations and two GP populations, to study the onset and control mechanisms of parkinsonian oscillations. A theoretical formula was obtained for generating oscillations without internal globus pallidus connections. Based on this formula, we analysed the effects of the cortex inputs, striatum inputs, coupling weights and delays on the conditions of beta oscillation generations and found that the theoretical results basically agree with the numerical results in the changing trend, and the internal globus pallidus connection has little effect on oscillations. The onset mechanism can be explained by the model itself. Finally, we compared the oscillation conditions to those in previous studies and found that the delays and coupling weights required for generating oscillations might decrease as the number of nuclei increases. As the data listed in the "Appendix" were all derived from experiments, theoretical analysis and numerical simulation compared well in this model, we hope that the results obtained can inspire further theoretical and experimental studies.

The model we propose is discussed in "The model introduced" section; the theoretical derivation of oscillatory conditions is detailed in "Derivation of oscillatory conditions" section; the method we used for numerical simulation is presented in "Numerical simulation method" section; effects of the cortex output, the striatum output, the delay and coupling strengths on oscillations are discussed in "The effects of various factors on oscillatory conditions" section; finally, results are discussed in "Discussion" section.

The model introduced

The newly built STN–GP network model is shown in Fig. 1. It contains two STN neural populations (STN1 and STN2) and two GPe neural populations (GP1 and GP2). The arrows represent excitatory projections mediated by glutamate, and lines ending with solid dots are inhibitory inputs adjusted by aminobutyric acid. The GP1 and GP2 populations also contain internal inhibitory self-feedback connections. The cortex output (C) to the STN1 and the striatum output (S) to the GP1 are taken as constants in our study. "W" represents the coupling strength between different neural populations. For example, W_{GS} is the strength of the connection from the GP to the STN. "T" denotes the signal transmission delay in the pathway.

Now, we use the mean firing-rate equations (Dayan and Abbott 2001; Vogels et al. 2005; Holgado et al. 2010;

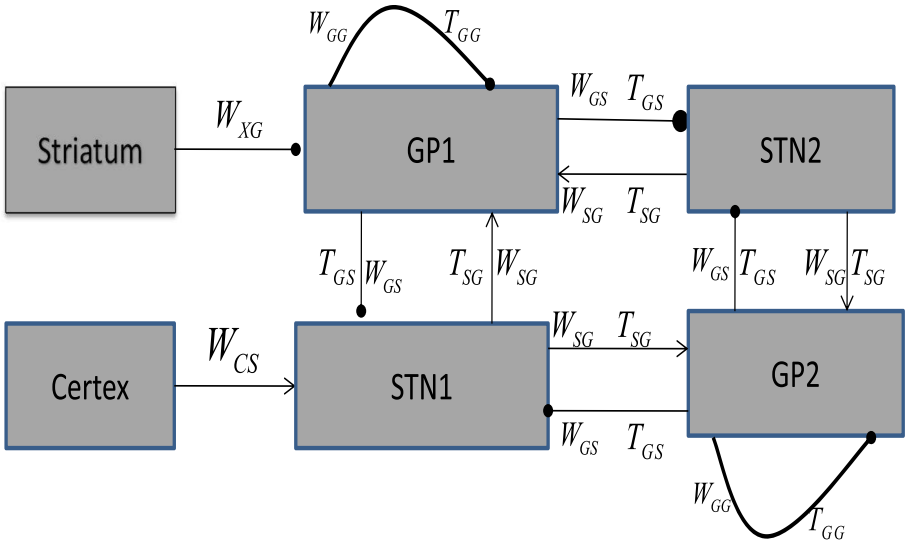

Fig. 1 Schematic of the STN–GP network model. It contains two STN populations and two GPe populations, and the cortex and striatum inputs are taken as constants in this paper. Arrows represent excitatory projections mediated by glutamate, and round dots indicate the mean inhibitory connections adjusted by aminobutyric acid. W and T represent the coupling strengths and delays on each pathway, respectively

Pavlides et al. 2012) to describe the network model in Fig. 1,

$$\tau_s S_1'(t) = F_s(-w_{GS}G_1(t-T_{GS}) - w_{GS}G_2(t-T_{GS}) + w_{CS}Ctx) - S_1(t) \quad (1)$$

$$\tau_s S_2'(t) = F_s(-w_{GS}G_1(t-T_{GS}) - w_{GS}G_2(t-T_{GS})) - S_2(t) \quad (2)$$

$$\tau_G G_1'(t) = F_G(w_{SG}S_1(t-T_{SG}) + w_{SG}S_2(t-T_{SG}) - w_{XG}Str) - G_1(t) \quad (3)$$

$$\tau_G G_2'(t) = F_G(w_{SG}S_1(t-T_{SG}) + w_{SG}S_2(t-T_{SG})) - G_2(t) \quad (4)$$

Here, $S_1(t), S_2(t), G_1(t)$ and $G_2(t)$ are the mean firing rates of STN_1, STN_2, GP_1 and GP_2, respectively. $G_1(t-T_{GS})$, $G_2(t-T_{GS})$, $S_1(t-T_{SG})$ and $S_2(t-T_{SG})$ are the corresponding delayed firing rates. τ_s and τ_G are the time constants of the STN and GP populations, respectively. $F_s(.)$ and $F_G(.)$ represent the activation functions of the STN and GP, respectively, and describe the firing rate as a function of the synaptic inputs "x" (Holgado et al. 2010; Pavlides et al. 2012),

$$F_s(x) = \frac{M_s}{1 + (\frac{M_s - B_s}{B_s})exp(-4x/M_s)} \quad (5)$$

$$F_G(x) = \frac{M_G}{1 + (\frac{M_G - B_G}{B_G})exp(-4x/M_G)} \quad (6)$$

Here, M_S and M_G are the maximum firing rates, and B_s and B_G represent two basic discharge rates without external inputs. Figure 2a is a schematic diagram of the above activation functions (Pavlides et al. 2012). They are both sigmoid functions, which ensures that the mean firing rate will not exceed the maximum value. Figure 2b is the derivative of the corresponding activation functions (Pavlides et al. 2012), implying that the mean firing rate will not change quickly.

Figure 3a, b describe two different states of the brain obtained by setting C = 17 spk/s, S = 20 spk/s (a) and C = 30 spk/s, S = 6 spk/s (b). In the normal state, the firing rates of populations converge to constants; in the parkinsonian state, the firing rates show periodic synchronous oscillation phenomena.

To simplify the theoretical analysis, we suppose that all delays and time constants are equal, denoted as T and τ, respectively, in the following.

Derivation of oscillatory conditions

First, we analysed a linear system without cortical and striatal inputs,

$$\tau S_1'(t) = -w_{GS}G_1(t-T) - w_{GS}G_2(t-T) - S_1(t) \quad (7)$$

$$\tau S_2'(t) = -w_{GS}G_1(t-T) - w_{GS}G_2(t-T) - S_2(t) \quad (8)$$

$$\tau G_1'(t) = w_{SG}S_1(t-T) + w_{SG}S_2(t-T) - G_1(t) \quad (9)$$

$$\tau G_2'(t) = w_{SG}S_1(t-T) + w_{SG}S_2(t-T) - G_2(t) \quad (10)$$

Clearly, Eqs. (7)–(10) can be rearranged as

$$\begin{bmatrix} S_1'(t) \\ S_2'(t) \\ G_1'(t) \\ G_2'(t) \end{bmatrix} + A \begin{bmatrix} S_1(t-T) \\ S_2(t-T) \\ G_1(t-T) \\ G_2(t-T) \end{bmatrix} + B \begin{bmatrix} S_1(t) \\ S_2(t) \\ G_1(t) \\ G_2(t) \end{bmatrix} = 0 \quad (11)$$

where

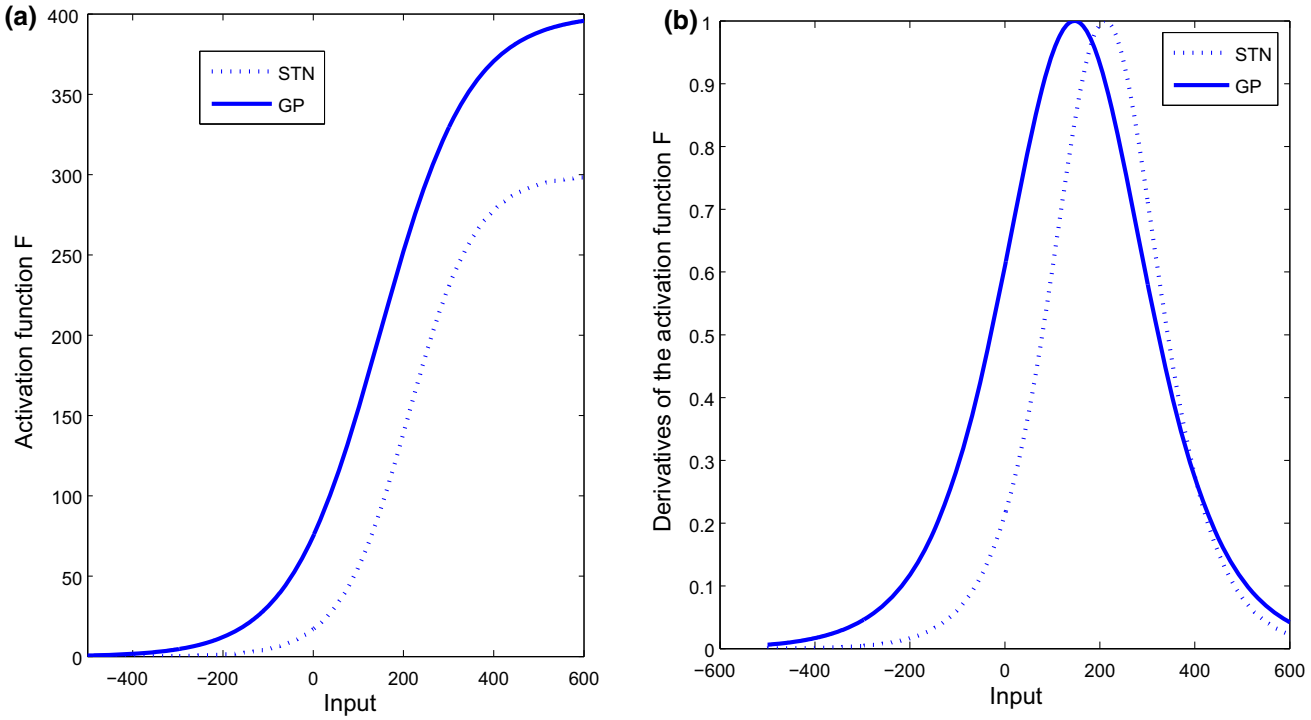

Fig. 2 **a** The activation functions $F_s(.)$ and $F_G(.)$, which are two sigmoid curves. **b** The derivatives of the activation functions, taken in [0,1]

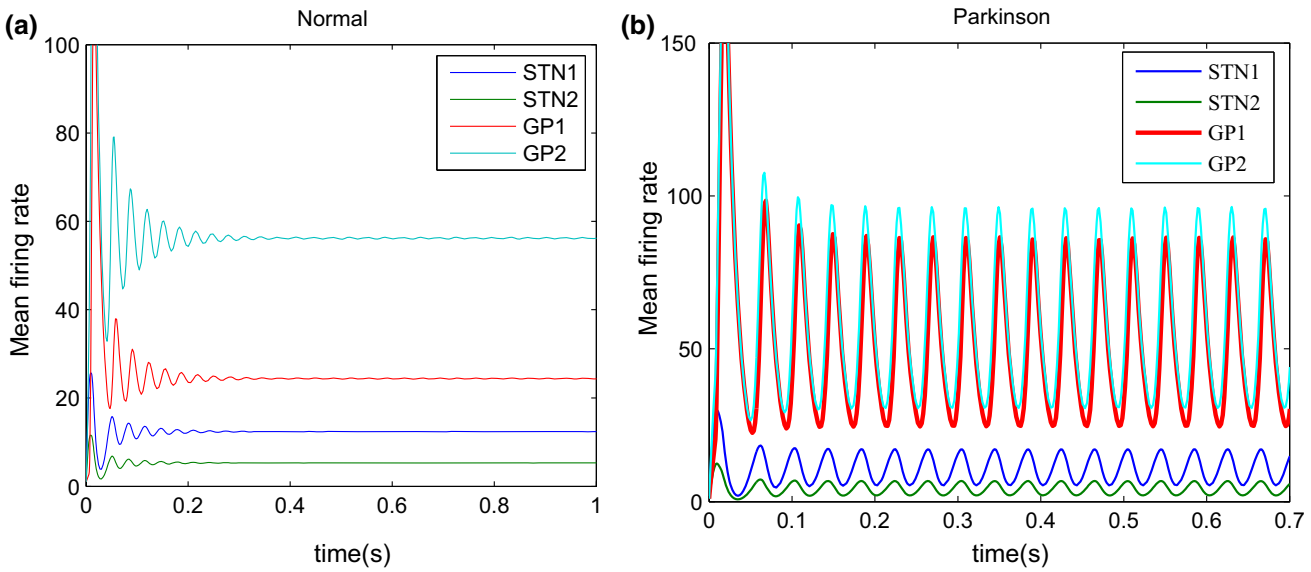

Fig. 3 Schematic diagrams of the normal state (**a**) and parkinsonian state (**b**) of the model. In the normal state, the mean firing rates of the populations converge to fixed points. In the parkinsonian state, four nerve nuclei show synchronous oscillations around fixed points. In the simulations, we set C = 17 spk/s, S = 20 spk/s (**a**) and C = 30 spk/s, S = 6 spk/s (**b**), respectively

$$A=\begin{bmatrix} 0 & 0 & \frac{w_{GS}}{\tau} & \frac{w_{GS}}{\tau} \\ 0 & 0 & \frac{w_{GS}}{\tau} & \frac{w_{GS}}{\tau} \\ \frac{-w_{SG}}{\tau} & \frac{-w_{SG}}{\tau} & 0 & 0 \\ \frac{-w_{SG}}{\tau} & \frac{-w_{SG}}{\tau} & 0 & 0 \end{bmatrix}$$
$$B=\begin{bmatrix} \frac{1}{\tau} & 0 & 0 & 0 \\ 0 & \frac{1}{\tau} & 0 & 0 \\ 0 & 0 & \frac{1}{\tau} & 0 \\ 0 & 0 & 0 & \frac{1}{\tau} \end{bmatrix} \quad (12)$$

In the following, we solved Eq. 11 mainly using the first shifting theorem of Laplace transforms (Schiff 2013),

$$L\{f(t-T)\}=e^{-TS}F(S) \quad (13)$$

and obtained

$$-\begin{bmatrix} S_1(0) \\ S_2(0) \\ G_1(0) \\ G_2(0) \end{bmatrix}+s\begin{bmatrix} S_1(s) \\ S_2(s) \\ G_1(s) \\ G_2(s) \end{bmatrix}+Ae^{-sT}\begin{bmatrix} S_1(s) \\ S_2(s) \\ G_1(s) \\ G_2(s) \end{bmatrix}+B\begin{bmatrix} S_1(s) \\ S_2(s) \\ G_1(s) \\ G_2(s) \end{bmatrix} = 0 \quad (14)$$

Without loss of generality, we assume that the initial condition is

$$\begin{bmatrix} S_1(0) \\ S_2(0) \\ G_1(0) \\ G_2(0) \end{bmatrix}=0$$

i.e.,

$$sI+Ae^{-sT}+B=0 \quad (15)$$

Thus, the characteristic equation of the variable "s" is obtained by taking the determinant on both sides of Eq. 15),

$$det(sI+Ae^{-sT}+B)=0 \quad (16)$$

According to the knowledge of ordinary differential equations (ODEs), the stability of the system is determined by the sign of the real part of the eigenvalue "s". If the real part of "s" is less than zero, the system is stable; otherwise, the system is unable. That is, when the real part equals zero, this condition generates oscillations. To facilitate the analysis, we substitute $s=i\lambda$ into Eq. 16 and carry out the exponential expansion,

$$-\lambda^2+\frac{1}{\tau^2}+\frac{2i\lambda}{\tau}+\frac{4}{\tau^2}w_{GS}w_{SG}(cos2\lambda T-isin2\lambda T)=0$$

By setting the real and imaginary parts to zero, we obtain

$$-\lambda^2+\frac{1}{\tau^2}+\frac{4}{\tau^2}w_{GS}w_{SG}cos2\lambda T=0 \quad (17)$$

$$\frac{2\lambda}{\tau}-\frac{4}{\tau^2}w_{GS}w_{SG}sin2\lambda T=0 \quad (18)$$

By squaring and adding (17) and (18), we find that

$$\lambda=\frac{\sqrt{4w_{GS}w_{SG}-1}}{\tau} \quad (19)$$

Finally, we substitute Eq. 19 back into Eq. 17 to give a final expression linking all parameters involved,

$$\frac{T}{\tau}=\frac{1}{2\sqrt{4w_{GS}w_{SG}-1}}\arccos\left(1-\frac{1}{2w_{GS}w_{SG}}\right)$$

i.e., the oscillation condition for the linear system is given by

$$\frac{T}{\tau}>\frac{1}{2\sqrt{4w_{GS}w_{SG}-1}}\arccos\left(1-\frac{1}{2w_{GS}w_{SG}}\right) \quad (20)$$

When Eqs. (1)–(4) include the sigmoid activation functions, the calculations become more complicated. First, we perform further analysis by linearizing the system at the fixed points $(S_1^*, S_2^*, G_1^*, G_2^*)$ to obtain an approximate linearized system (ALS). Then, the characteristic equation of ALS can also be obtained by employing a method similar to the above,

$$sI+A_1e^{-sT}+B=0$$
$$det(sI+A_1e^{-sT}+B)=0$$

where

$$A_1=\begin{bmatrix} 0 & 0 & F'_{S_1^*}\frac{w_{GS}}{\tau} & F'_{S_1^*}\frac{w_{GS}}{\tau} \\ 0 & 0 & F'_{S_2^*}\frac{w_{GS}}{\tau} & F'_{S_2^*}\frac{w_{GS}}{\tau} \\ -F'_{G_1^*}\frac{w_{SG}}{\tau} & -F'_{G_1^*}\frac{w_{SG}}{\tau} & 0 & 0 \\ -F'_{G_2^*}\frac{w_{SG}}{\tau} & -F'_{G_2^*}\frac{w_{SG}}{\tau} & 0 & 0 \end{bmatrix}$$
$$B=\begin{bmatrix} \frac{1}{\tau} & 0 & 0 & 0 \\ 0 & \frac{1}{\tau} & 0 & 0 \\ 0 & 0 & \frac{1}{\tau} & 0 \\ 0 & 0 & 0 & \frac{1}{\tau} \end{bmatrix} \quad (21)$$

and the derivatives of the activation functions in matrix A_1 can be written as

$$F'_{S_1^*} = F'_{S_1}(-w_{GS}G_1^* - w_{GS}G_2^* + w_{CS}Ctx) \quad (22)$$

$$F'_{S_2^*} = F'_{S_2}(-w_{GS}G_1^* - w_{GS}G_2^*) \quad (23)$$

$$F'_{G_1^*} = F'_{G_1}(w_{SG}S_1^* + w_{SG}S_2^* - w_{XG}Str) \quad (24)$$

$$F'_{G_2^*} = F'_{G_2}(w_{SG}S_1^* + w_{SG}S_2^*) \quad (25)$$

Finally, the approximate oscillation condition for the model in Fig. 1 is described as follows:

$$\frac{T}{\tau} = \frac{\arccos\left(1 - \frac{2}{(F'_{S_1^*}F'_{G_1^*} + F'_{S_1^*}F'_{G_2^*} + F'_{S_2^*}F'_{G_1^*} + F'_{S_2^*}F'_{G_2^*})w_{GS}w_{SG}}\right)}{2\sqrt{(F'_{S_1^*}F'_{G_1^*} + F'_{S_1^*}F'_{G_2^*} + F'_{S_2^*}F'_{G_1^*} + F'_{S_2^*}F'_{G_2^*})w_{GS}w_{SG} - 1}} \quad (26)$$

i.e., the model is oscillatory if and only if the parameters satisfy the following inequality:

$$\frac{T}{\tau} > \frac{\arccos\left(1 - \frac{2}{(F'_{S_1^*}F'_{G_1^*} + F'_{S_1^*}F'_{G_2^*} + F'_{S_2^*}F'_{G_1^*} + F'_{S_2^*}F'_{G_2^*})w_{GS}w_{SG}}\right)}{2\sqrt{(F'_{S_1^*}F'_{G_1^*} + F'_{S_1^*}F'_{G_2^*} + F'_{S_2^*}F'_{G_1^*} + F'_{S_2^*}F'_{G_2^*})w_{GS}w_{SG} - 1}}$$

Numerical simulation method

We mainly handled numerical results by using the DDE23 function in the MATLAB environment.

To find the oscillatory condition specified by Eq. (26), first, we must obtain fixed points of the system under different parameters, denoted by $(S_1^*, S_2^*, G_1^*, G_2^*)$. This can be realized by minimizing Eq. (27),

$$\begin{aligned} R = {} & (F_s(-w_{GS}G_1(t-T_{GS}) - w_{GS}G_2(t-T_{GS}) + w_{CS}Ctx) - S_1(t))^2 \\ & + (F_s(-w_{GS}G_1(t-T_{GS}) - w_{GS}G_2(t-T_{GS})) - S_2(t))^2 \\ & + (F_G(w_{SG}S_1(t-T_{SG}) + w_{SG}S_2(t-T_{SG}) - w_{XG}Str) - G_1(t))^2 \\ & + (F_G(w_{SG}S_1(t-T_{SG}) + w_{SG}S_2(t-T_{SG}) - G_2(t))^2 \end{aligned} \quad (27)$$

Then, $(S_1^*, S_2^*, G_1^*, G_2^*)$ is substituted into Eqs. (22), (23), (24) and (25) to obtain the values of $F'_{S_1^*}, F'_{S_2^*}, F'_{G_1^*}, F'_{G_2^*}$. Finally, oscillatory conditions are obtained by Eq. (26), as shown in Fig. 4a.

To analyse the type of oscillation generated in the model, we performed the power spectral analysis on the time series of GP_1 via the fast Fourier transform and took the maximum peak frequency as the dominant frequency (DF) of GP_1. We see that in the vicinity of the oscillatory conditions, the DF falls in the typical β band (12–30 Hz), as shown in Fig. 4b, which is one of the critical clinical features of Parkinson's disease. Moreover, in some oscillating regions, other types of parkinsonian oscillations also appear, such as the typical static tremor (4–6 Hz) in Fig. 5e. To help us better understand the oscillation mechanism, we also simulated the mean discharge rates (MD) of the GP1, such as Fig. 4c, which represents the firing activation level of populations. The MD changes with changing of the coupling strengths and delays in this model. Unless otherwise noted, the parameters employed in the simulations, which are all listed in the "Appendix", originated from real physiological experiments. It should be noted that we selected the GP1 as a representative in the following computational simulations because the oscillatory activities of different populations are synchronous.

The effects of various factors on oscillatory conditions

Figure 4a describes the effect of cortex inputs (C) on the generation of oscillations. The system is oscillatory (OS) when parameters fall into the region above the curve. When $\frac{T}{\tau}$ is fixed, increasing the cortex inputs can push the system from normal states (NS) to oscillating states, as indicated by the arrow. This onset mechanism can be explained directly from the model itself. The firing activation level of the STN1 increased as C increased, which in turn improved the firing activation level of the GP1 through the excitatory pathway "$STN1 \rightarrow GP1$". Therefore, the state of the GP1 evolved from the stable state to the oscillating state, and the mean discharge rates increased gradually, as shown in Fig. 4c. By calculating the dominant frequency of the GP1, we found that frequencies near oscillatory conditions mainly fall in the range of 13–30 Hz, which is the typical parkinsonian oscillation β band, as shown in Fig. 4b. Moreover, as C increases further, some other oscillating frequency bands appear, such as the typical static tremor (4–6 Hz). To see these oscillation phenomena in Fig. 4b, c more clearly, we simulated four specific time sequence diagrams, shown in Fig. 4d–g, which were obtained by setting C = 39 , C = 59, C = 100 and C = 200, respectively. The analytical result (Eq. 26) and the simulation result (red asterisks) fit very well. In addition, we may also explain the oscillation generation mechanism by Eq. (26). From Eq. (26), we can see that, to ensure the occurrence of oscillatory activity, the terms T/τ and $F'_{S_1^*}F'_{G_1^*} + F'_{S_1^*}F'_{G_2^*} + F'_{S_2^*}F'_{G_1^*} + F'_{S_2^*}F'_{G_2^*}$ must both be sufficiently large. On the other hand, as C increased, the values of $F'_{S_1^*}F'_{G_1^*} + F'_{S_1^*}F'_{G_2^*} + F'_{S_2^*}F'_{G_1^*} + F'_{S_2^*}F'_{G_2^*}$ also increased, as shown in Fig. 4h. Therefore, the state in which the GP1 transferred from the NS to the OS is shown in Fig. 4a.

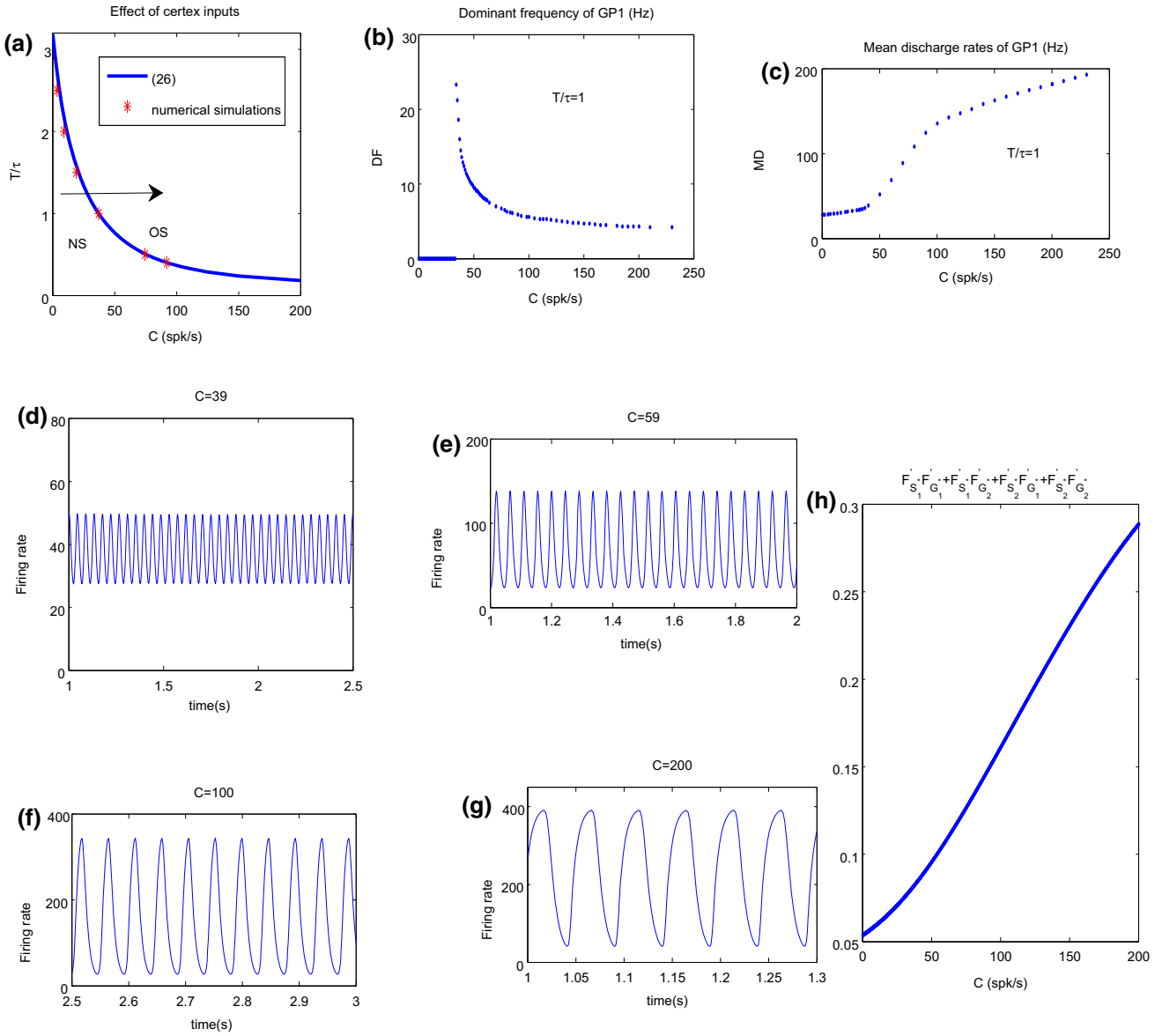

Fig. 4 **a** The effect of C on the generation of oscillations. The system is oscillatory (OS) when the parameters fall into the region above the curve. When T is fixed, increasing C can push the system from the normal state (NS) to the OS, as indicated by the arrow. The analytical result (Eq. 26) and the simulation result (red asterisks) fit very well. **b**, **c** The DF and MD of the GP_1, respectively. With increasing C, the DF decreased gradually, while the MD increased. **d**–**g** Four specific time sequence diagrams of the GP_1 corresponding to (**b**) and (**c**), obtained by setting C = 39 , C = 59, C = 100 and C = 200, respectively. **h** The change in $F'_{S_1^*}F'_{G_1^*} + F'_{S_1^*}F'_{G_2^*} + F'_{S_2^*}F'_{G_1^*} + F'_{S_2^*}F'_{G_2^*}$ with increasing C. In all simulations, we set S = 12 spk/s and $\tau = 0.006$ s

The striatum mainly exerts inhibitory projections to the GP1 in the model, which may lead to a decrease in the activation level of the GP1. Figure 5a is an oscillating condition graph affected by striatum inputs, and Fig. 5b is a local enlarged image. Through calculation, we know that the minimal value of $\frac{T}{\tau}$ on the oscillatory condition curve is approximately 2.045, and with increasing of striatum inputs, $\frac{T}{\tau}$ tends to a constant(approximately 2.191) on the horizontal line in Fig. 5a. Clearly, when $\frac{T}{\tau}$ was fixed between approximately 2.045 and 2.191, increasing the striatal inputs first pushed the GP1 from a stable state to an oscillating state and then again into a stable state, as shown by the double arrow. From the model in Fig. 1, we can see that the excitatory pathway "$STN1 \rightarrow GP1$" is the main direct pathway that promotes increasing the activation level of the GP1. Therefore, to ensure the production of the GP1 oscillations, the firing ability of the STN1 must be sufficiently strong. In other words, the inhibitory effect from the GP1 must be sufficiently weak. When the striatum input began to increase, it mainly reduced the inhibitory outputs from the GP1 to the STN1, and oscillations occurred in and

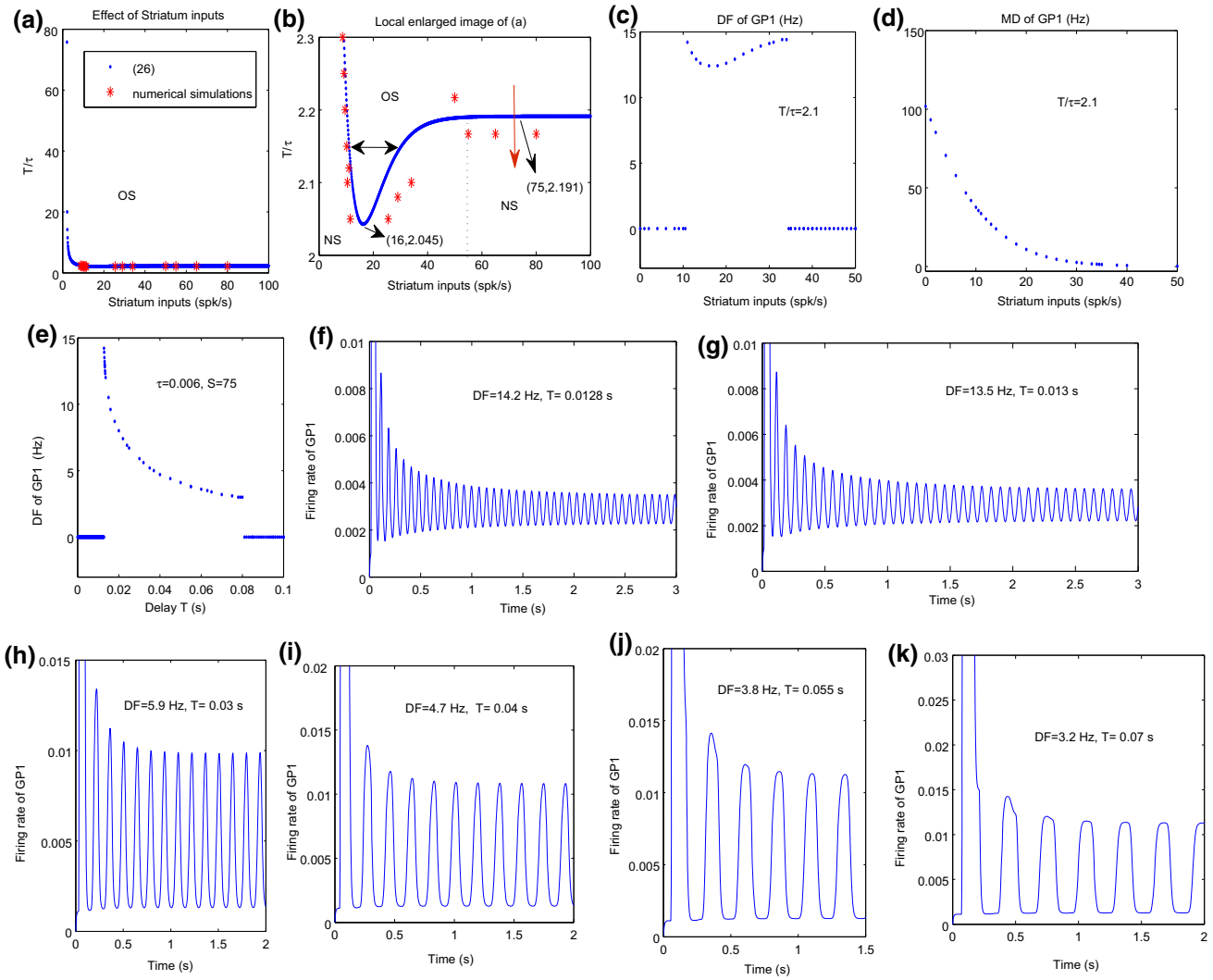

Fig. 5 The effect of S on the onset of oscillations. C is fixed at 10 spk/s. **a** The system is oscillatory when the parameters fall into the region above the curve, denoted as "OS". The analytical and numerical simulation results basically coincide, and the simulation results were obtained by setting $\tau = 0.006$ s. When T/τ is sufficiently large (> 2.2), increasing S can push the system from the NS to the OS. **b** The local enlarged image of (**a**) with the T/τ fixed in the interval [2,2.3], which shows that the oscillation state can be inhibited by increasing or decreasing S, as indicated by the double arrow, and T/τ required sufficiently large (> 2.045) to ensure the onset of oscillation activity. Moreover, when the S is large enough (> 55), oscillations occur only when the T/τ exceeds 2.191, as shown by the red arrow. **c**, **d** The DF and MD of the GP1, obtained by setting $\tau = 0.006$ s and $T/\tau = 2.1$. They show that the DF near the oscillatory condition area falls in the beta band, and the MD decreases with increasing S. **e** The change in the DF of the GP1 with increasing the delay T, which was obtained by fixing S = 75 spk/s and $\tau = 0.006$ s in (**b**). We found that oscillatory activities occurred when T was large enough, and different frequency bands, such as the beta frequency band (13–30 Hz) and the resting tremor (4–6 Hz), appeared with further increases in T. Finally, the oscillation phenomenon disappeared when the delay was too large. **f**–**k** Six specific time sequence diagrams corresponding to (**e**), obtained by setting T = 0.0128 s, T = 0.013 s, T = 0.03 s, T = 0.04 s, T = 0.055 s and T = 0.07 s, respectively

GP1; however, when the striatum input increased to too large a value, the oscillation activities of the GP1 were inhibited. This phenomenon can also be understood from the viewpoint of numerical calculations. Figure 6 describes the change in the derivative values of $F'_{S_1^*}F'_{G_1^*} + F'_{S_1^*}F'_{G_2^*} + F'_{S_2^*}F'_{G_1^*} + F'_{S_2^*}F'_{G_2^*}$ with increasing of striatum inputs S, which implies that $F'_{S_1^*}F'_{G_1^*} + F'_{S_1^*}F'_{G_2^*} + F'_{S_2^*}F'_{G_1^*} + F'_{S_2^*}F'_{G_2^*}$ first increased to a sufficiently large value to ensure oscillation generation and then decreased to a sufficiently small value to make the oscillations disappear. In Fig. 7, we concretely calculated the values of $F'_{S_1^*}, F'_{S_2^*}, F'_{G_1^*}, F'_{G_2^*}$ with various striatum inputs and with the striatum inputs taken as 5 spk/s, 15 spk/s, 40 spk/s in Fig. 7a–c, respectively. In Fig. 7a, the striatum input is relatively small, and from Fig. 1, we can intuitively infer that the inhibitory inputs into the GP1 are small, and in turn, the inhibitory projections from the Gp1 to the other populations become

relatively large, i.e., the system is generally inhibited now, and the term $F'_{S_1^*}F'_{G_1^*} + F'_{S_1^*}F'_{G_2^*} + F'_{S_2^*}F'_{G_1^*} + F'_{S_2^*}F'_{G_2^*}$ is too small (approximately 0.0531) to induce oscillations. However, in Fig. 7b, the striatum input is relatively large, and its inhibitory action on the GP1 is increased; in turn, the inhibitory outputs from the GP1 to the other populations are decreased, and therefore, the relative effects of the cortex on the excitability of the system are enhanced, i.e., the term $F'_{S_1^*}F'_{G_1^*} + F'_{S_1^*}F'_{G_2^*} + F'_{S_2^*}F'_{G_1^*} + F'_{S_2^*}F'_{G_2^*}$ is now sufficiently large (approximately 0.0602) to induce oscillations. Moreover, with further increasing of the striatal inputs, as shown in Fig. 7c, the inhibitory projections from the striatum to the Gp1 are too large in this case, which causes the system to be inhibited overall, and the term $F'_{G_1^*}$ becomes too small(approximately 0.0054) to induce oscillations. From Fig. 5a, b, we can see that the theoretical result (26) and the numerical simulation results compare very well, at least in terms of the change trend. Figure 5c, d show the DF and MD of the GP1 with increasing S, respectively. Here, we set $T/\tau = 2.1$. The DF of the GP1 in the oscillation region is 13–15 Hz. The increase in S can reduce the firing activation level of the GP1; therefore, the MD decreases gradually in Fig. 5d. Figure 5e shows the change trend of the DF when S is fixed at 75 spk/s, where oscillations appear only when the delay is sufficiently large. We know that if the striatal inputs are too large, the system is inhibited. However, we might infer that delays could alleviate this inhibition effect, such as in the pathway

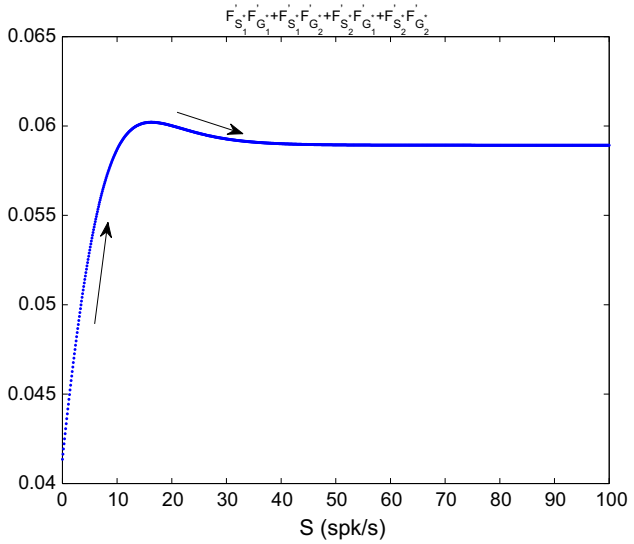

Fig. 6 The values of $F'_{S_1^*}F'_{G_1^*} + F'_{S_1^*}F'_{G_2^*} + F'_{S_2^*}F'_{G_1^*} + F'_{S_2^*}F'_{G_2^*}$ as a function of S. It is shown that the function value first increases and then decreases, which implies that the system transfers from the NS to the OS with increasing S. If the S is too large, the OS may also disappear. In the simulations, the parameters were the same as in Fig. 5a

"*Striatum* → *GP*1 → *STN*1". Therefore, the relative excitatory projections from the STN1 and STN2 increased, and oscillations occurred with increasing delays. In Fig. 8, we simulated the MD of four populations with increasing of delays. The MD of the four populations increased gradually when the delay was sufficiently large. It should also be noted that the oscillations disappeared if the delay increased to too great a value, as shown in Fig. 5e. This may be because the excitatory projections from the STN1 and STN2 to the GP1 lagged too long. Figure 5f–k are six specific time sequence diagrams corresponding to Fig. 5e, obtained by setting T = 0.0128 s, T = 0.013 s, T = 0.03 s, T = 0.04 s, T = 0.055 s and T = 0.07 s, respectively. They show that the DF of the GP1 decreased with increasing T, and some typical types of Parkinson oscillation appeared, such as the β frequency band (13–30 Hz) and the static tremor frequency band (4–6 Hz).

Figure 9a, b show the effect of the coupling strength W_{SG} on the generation of oscillations. On the one hand, if T/τ is fixed as a constant, increasing W_{SG} can push the GP1 from the stable state to the oscillation state. This effect can be easily explained from the model itself. W_{SG} is the excitatory coupling strength projected from the STN to the GP1, and its increase can enhance the activation level of the GP1, causing the state of the GP1 to transfer from the NS to the OS. The MD of the GP1 also increased, as shown in Fig. 9c. In addition, the DF of the GP1 decreased from the typical beta band to some other frequency ranges, such as the static tremor (4–6 Hz). However, to ensure the occurrence of oscillations, the delay must be sufficiently large, as shown in Fig. 9a, b. Moreover, when W_{SG} increased to a relatively large value, as shown in the right side of Fig. 9a, b, the onset of oscillations depends only on T. It is an interesting problem and might be explained as follows. If T is too small, then the signal transmission along the closed loops "*STN*1 → *GP*1 → *STN*1" and "*STN*2 → *GP*1 → *STN*2" is very quick. However, W_{SG} is the direct excitatory coupling strength projected from the STN1 and STN2 to the GP1, which may in turn be inhibited quickly by the inhibitory pathways "*GP*1 → *STN*1" and "*GP*1 → *STN*2". Therefore, the model requires large enough delays to generate oscillations. Figure 9e, f show the changes in the DF and MD of the GP1 as the delay T increases, obtained by fixing both $W_{SG} = 50$ and $\tau = 0.006$ s in Fig. 9b. We found that oscillatory activities occurred when T increased to a sufficiently large value (> 0.0044 s). The MD increased and different frequency bands appeared with further increases in T. Figure 9g–j are four specific time sequence diagrams corresponding to Fig. 9f, obtained by setting T = 0.0045 s, T = 0.005 s, T = 0.012 s and T = 0.017 s, respectively. Figure 9g, h show typical β oscillations, and Fig. 9i, j show typical resting tremor phenomena.

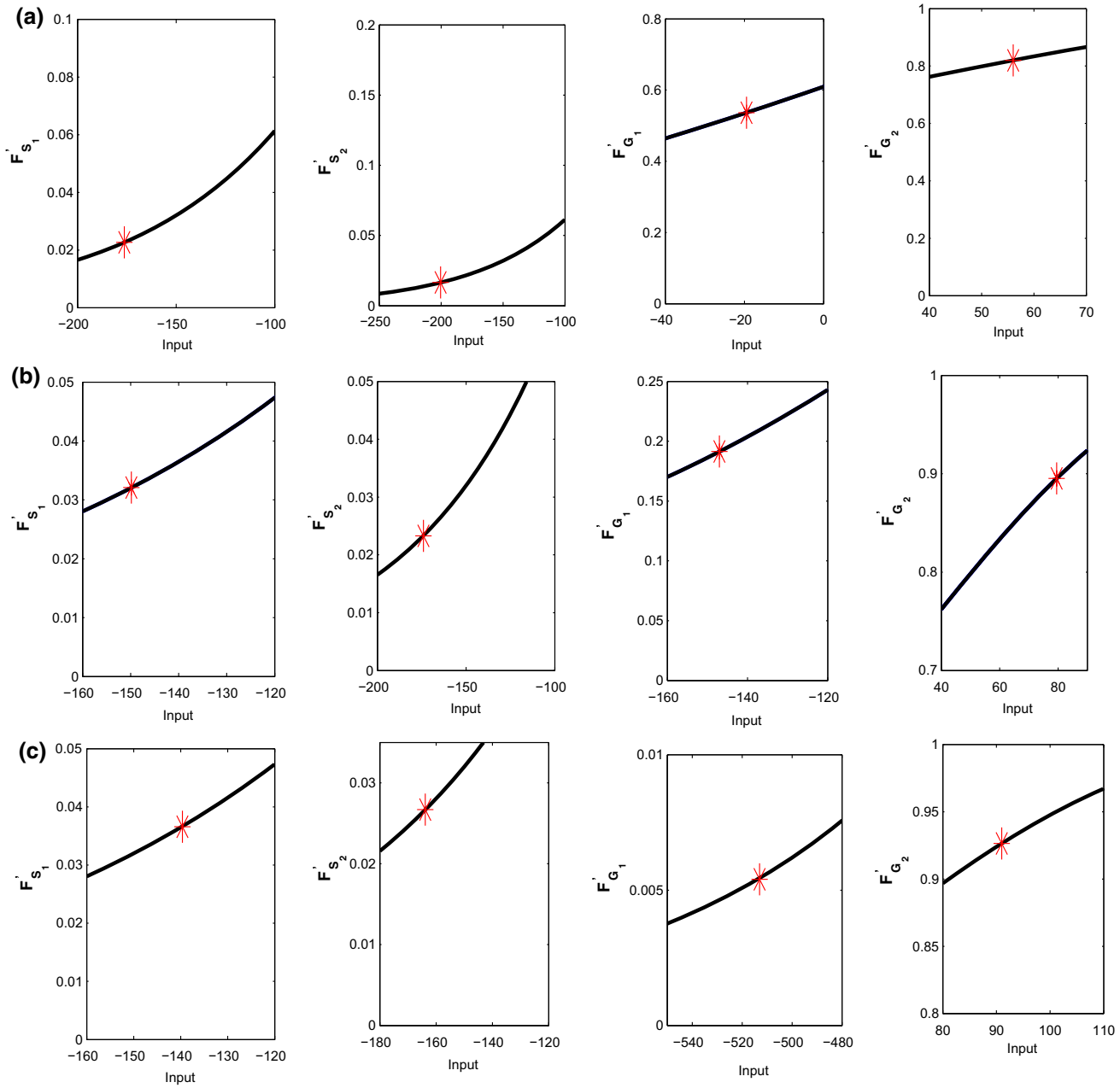

Fig. 7 Specific calculation results of the term $F'_{S_1^*}F'_{G_1^*} + F'_{S_1^*}F'_{G_2^*} + F'_{S_2^*}F'_{G_1^*} + F'_{S_2^*}F'_{G_2^*}$ corresponding to Fig. 5b. Here, the C was set to 10 spk/s. The S was set to 5 spk/s, 15 spk/s and 40 spk/s in (**a**–**c**), respectively. Red asterisks are the values of the derivatives of the activation functions. In (**a**), $F'_{S_1^*}F'_{G_1^*} + F'_{S_1^*}F'_{G_2^*} + F'_{S_2^*}F'_{G_1^*} + F'_{S_2^*}F'_{G_2^*}$ is too small to induce oscillations; in (**b**), $F'_{S_1^*}F'_{G_1^*} + F'_{S_1^*}F'_{G_2^*} + F'_{S_2^*}F'_{G_1^*} + F'_{S_2^*}F'_{G_2^*}$ increased sufficiently to induce oscillations; in (**c**), the S projected to the Gp1 is too large, so the term $F'_{G_1^*}$ becomes too tiny to induce oscillations. (Color figure online)

W_{GS} is another coupling strength in the closed loop "$STN \rightarrow GP \rightarrow STN$", and its effect on the generation of oscillations is different from that of W_{SG}. As shown in Fig. 10a, oscillations are generated only when W_{GS} falls in a specific range, indicated by the double arrow. The DF of the GP1 in the oscillation region are mainly in the range of 13–30 Hz, as shown in Fig. 10b. Increasing W_{GS} will reduce the activation level of the STN1 and STN2, which in turn reduce the activation level of the GP1. Therefore, the MD of the GP1 decreased with increasing W_{GS}, as shown in Fig. 10c. Figure 10d describes the change trend of the derivative value $F'_{S_1^*}F'_{G_1^*} + F'_{S_1^*}F'_{G_2^*} + F'_{S_2^*}F'_{G_1^*} + F'_{S_2^*}F'_{G_2^*}$ with increasing W_{GS}. It first increases to push the state from the NS to the OS and then decreases to push the state from the OS to the NS, which agrees with the

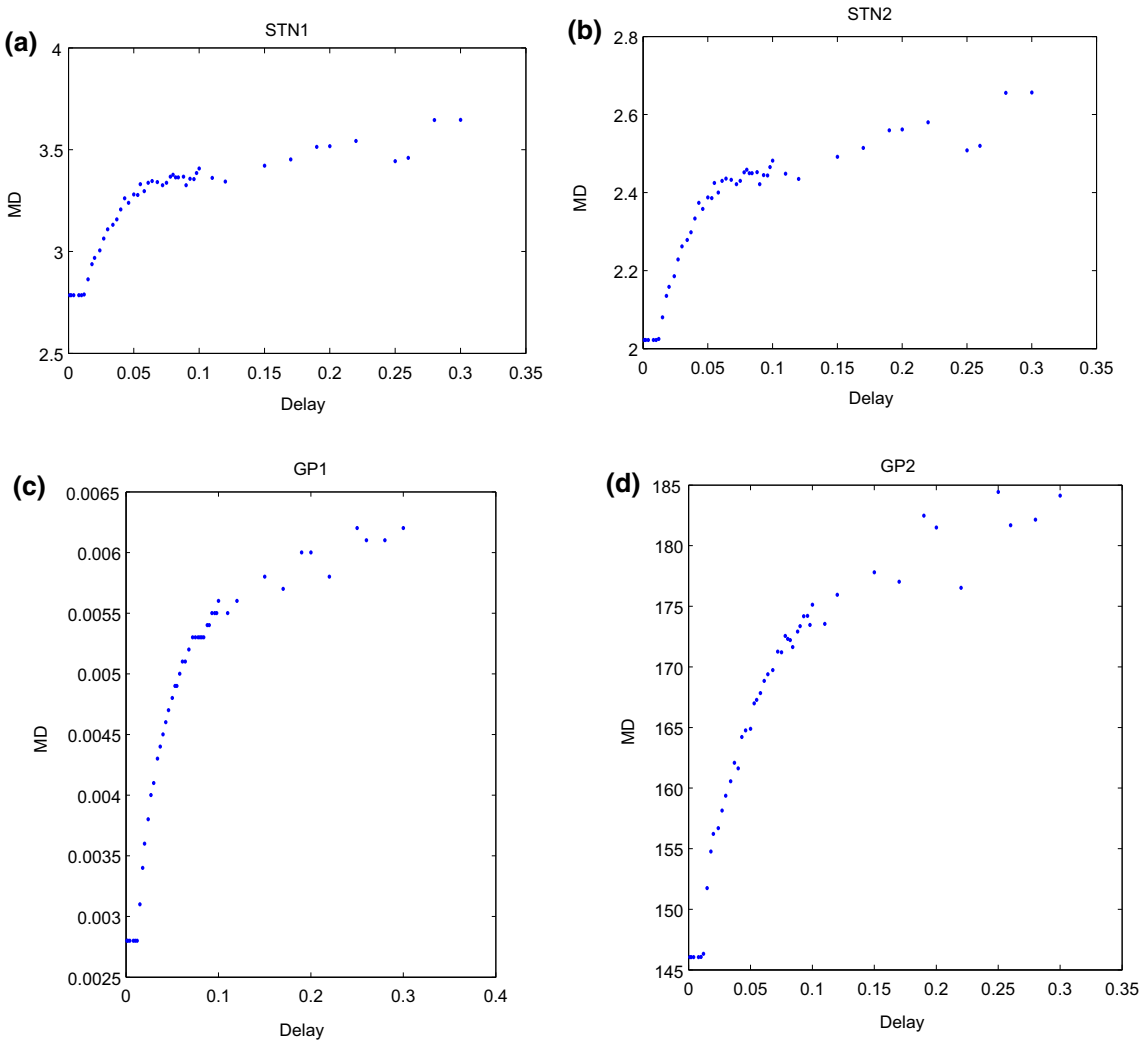

Fig. 8 The MD values of four populations, corresponding to Fig. 5e. They show that the activation level of the model increased with increasing delay when S becomes sufficiently large

analytical results of formula (26). On the other hand, in the oscillation region, if we keep W_{GS} constant, the occurrence of oscillations depends only on delays. Figure 10e, f are the DF and MD of the GP1 with increasing delays, both obtained by setting $w_{GS} = 0.8$. With increasing T, the MD increased, and different frequency bands of the parkinsonian oscillation appeared, such as the typical 13–30 Hz and 4–6 Hz. This result might be explained as follows. W_{GS} is the inhibitory coupling weight, and the model is stable if the W_{GS} is sufficiently large. In this case, the delay may relieve the inhibition of the pathway "$GP \rightarrow STN$", so the oscillatory activity appears again when the delay is sufficiently large, as shown in Fig. 10e, f.

It should be noted that the globus pallidus has an internal self-inhibitory feedback connection W_{GG}, which is omitted in the above theoretical derivations because it would lead to tedious calculations. Moreover, through the numerical simulation calculations shown in Fig. 11, we found that W_{GG} has little effect on oscillatory conditions, which agrees with the findings of some previous studies (Holgado et al. 2010; Pavlides et al. 2012).

Discussion

The hypokinetic symptoms of PD are related to excessive synchrony oscillations in the basal ganglia, especially the STN–GP network. However, there is as yet little theoretical research on the onset mechanism of PD. In this paper, we built a basal ganglia mean discharge rate model that contains the cortex, striatum, two STN populations and two GP populations to study the oscillatory conditions of Parkinson's disease. First, we obtained an approximate oscillation condition formula (26) from the Laplace transformation. Then, we considered the effects of some critical factors, such as the cortex outputs, the striatum outputs, the W_{GS},

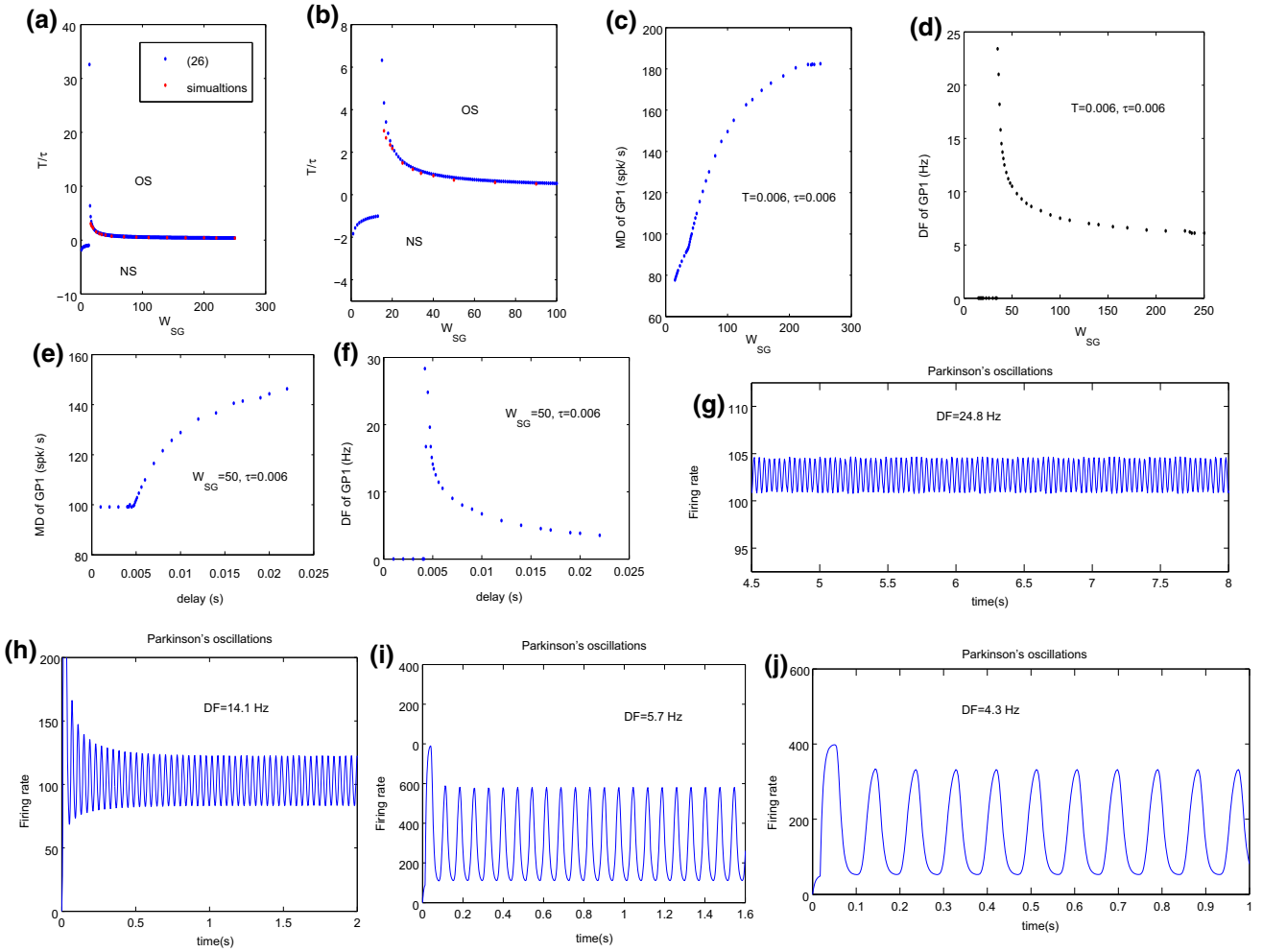

Fig. 9 The effect of the W_{SG} on oscillations. The C and S are fixed at 22 spk/s and 3 spk/s, respectively. **a** The system is oscillatory in the region above the curve, denoted as "OS". The analytical and simulation results basically coincide, and the simulation results were obtained by setting $\tau = 0.006$ s. When T/τ is a fixed constant, increasing W_{SG} can push the system from the NS to the OS. **b** A local enlarged image of (**a**) with the T/τ fixed in the interval [0,8]. The oscillations may only depend on delays when the W_{SG} is large enough, as shown on the right side of the figure. **c**, **d** The MD and DF of the GP1, obtained by setting $T/\tau = 1$. They show that the DF near the oscillatory condition falls into the beta band, and the MD increases with increasing W_{SG}. Moreover, with further increases in W_{SG}, oscillations appear in different frequency bands, such as the static tremor. **e**, **f** The DF and MD of the GP1 with increasing delay T, both obtained by fixing W_{SG}=50 and $\tau = 0.006$ s in (**b**). Oscillatory activities can be induced when T increases to a sufficiently large value (> 0.0044 s), and different frequency bands appear with further increases in T, such as the 13–30 Hz and 4–6 Hz oscillations. **g**–**j** Four time sequences corresponding to (**f**), obtained by setting T = 0.0045 s, T = 0.005 s, T = 0.012 s and T = 0.017 s, respectively. Where (**g**) and (**h**) are typical β oscillations, and (**i**) and (**j**) are typical resting tremor phenomena

the W_{SG} and delay, on oscillations. We found that the theoretical derivation result (26) and numerical simulation results compare well, as illustrated in Fig. 4a. The data listed in the "Appendix" were all derived from previous experiments. However, it remains to be further explored how well the analytical and numerical results obtained in this model agree with experiments. Moreover, the advantage of the oscillation condition (26) is easier analysis of the onset mechanism of oscillation conditions, as it shows the relationship of all the parameters in the model in one mathematical expression, as shown in Fig. 4h.

The cortex and striatum populations were simplified as constant inputs to the STN–GP network to facilitate the analytical deduction of oscillation conditions and focused mainly on the STN–GP circuits mechanisms to generate oscillations. Figures 4a and 5a indicated that cortex and striatum neurons may also exert great effects on oscillations. Some previous studies (Ahn et al. 2016) implied that the cortex was the origin of Parkinson's beta oscillations and that the cortex and STN–GP circuits mechanisms are not mutually exclusive, which provided some degree of reconciliation with our views. Of course, the more precise mechanisms of the effects of the cortex and striatum on

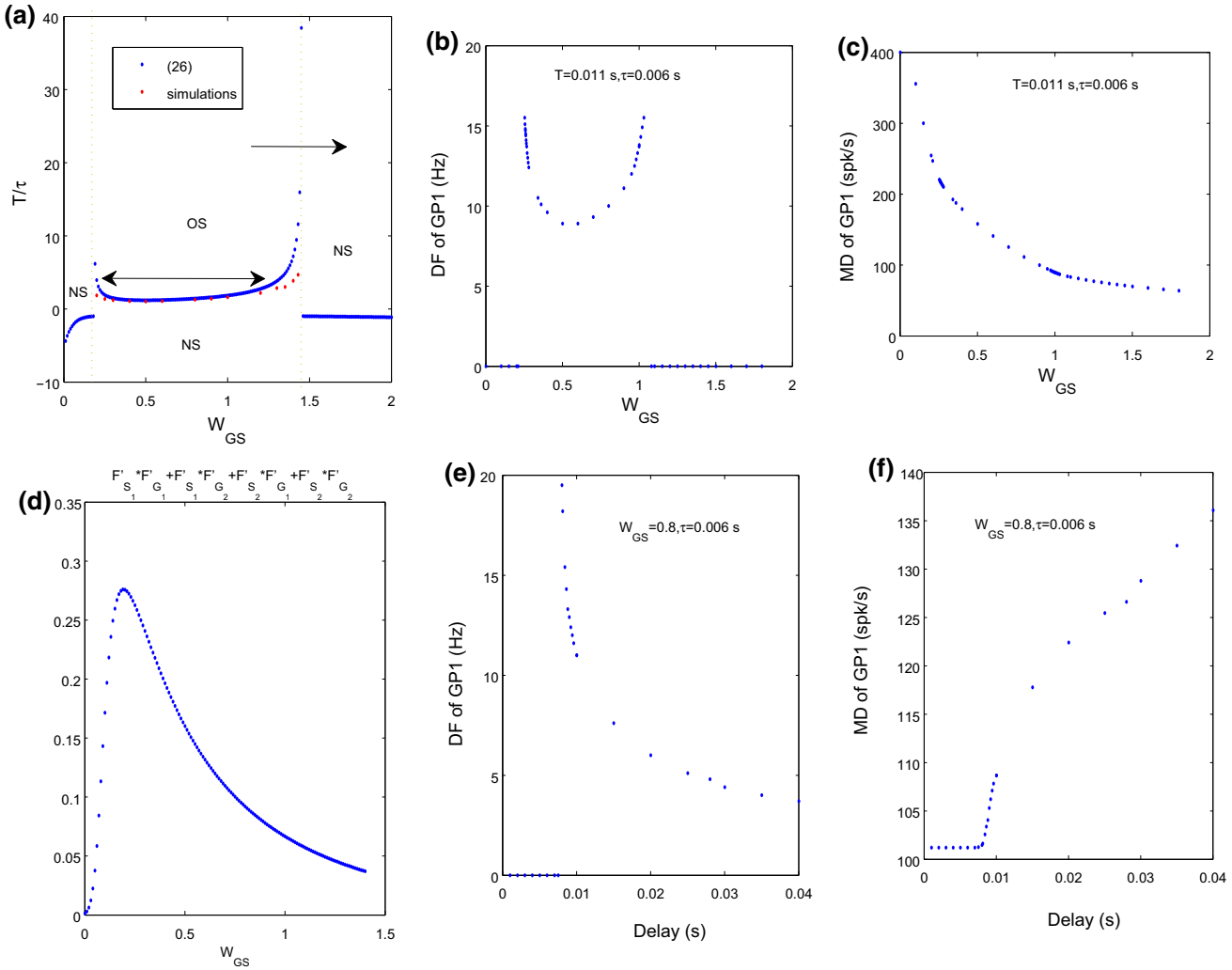

Fig. 10 The effect of the coupling strength W_{GS} on the generation of oscillations. **a** The system is oscillatory when parameters fall into the region denoted as "OS". The analytical and numerical simulation results compare well, and the simulation results were obtained by setting $\tau = 0.006$ s. When T/τ is a fixed constant, increasing or decreasing W_{GS} can both push the system from the OS to the NS, indicated by the double arrow. **b**, **c** The DF and MD of the GP1, obtained by setting $T = 0.011$ s and $\tau = 0.006$ s. **d** The change in derivative values $F'_{S_1}F'_{G_1} + F'_{S_1}F'_{G_2} + F'_{S_2}F'_{G_1} + F'_{S_2}F'_{G_2}$ with increasing W_{GS}. **e**, **f** The DF and MD of the GP1 with increasing delays, obtained by setting $w_{GS} = 0.8$ and $\tau = 0.006$ s. In all simulations, we used C = 22 spk/s, S = 3 spk/s and $w_{SG} = 20$

beta oscillations should be examined by the use of a more realistic brain network model in the future, such as the spiking model. We hope that the results obtained in this paper can provide a reference for further study.

To explain the relevant onset mechanisms, we simulated the DF and MD of the GP1 with variation in these parameters. The variation trends of the DF and MD are contrary, as shown in Fig. 10e, f. We might infer that the magnitude and dominant frequency of oscillations are inversely related to Parkinson's disease, which should be further confirmed experimentally. We found that the mechanism of oscillations can be well explained by the model itself together with the variation trends of the DF and MD. We also studied the effect of the W_{GG} on oscillations and found that its effect was small.

The first model showed beta oscillations directly derived from the STN–GP network developed by Holgado et al. (2010) and Pavlides et al. (2012) employed the same model to obtain an improved oscillating condition by using the Laplace transformation and found that the theoretical results compared very well with the numerical results. The model in this paper was developed from the above studies and contains two STN populations and two GP populations. We found that theoretical oscillation conditions also compared well with numerical simulation results in this model. In addition, we found some new phenomena that have not been emphasized in previous studies. In addition

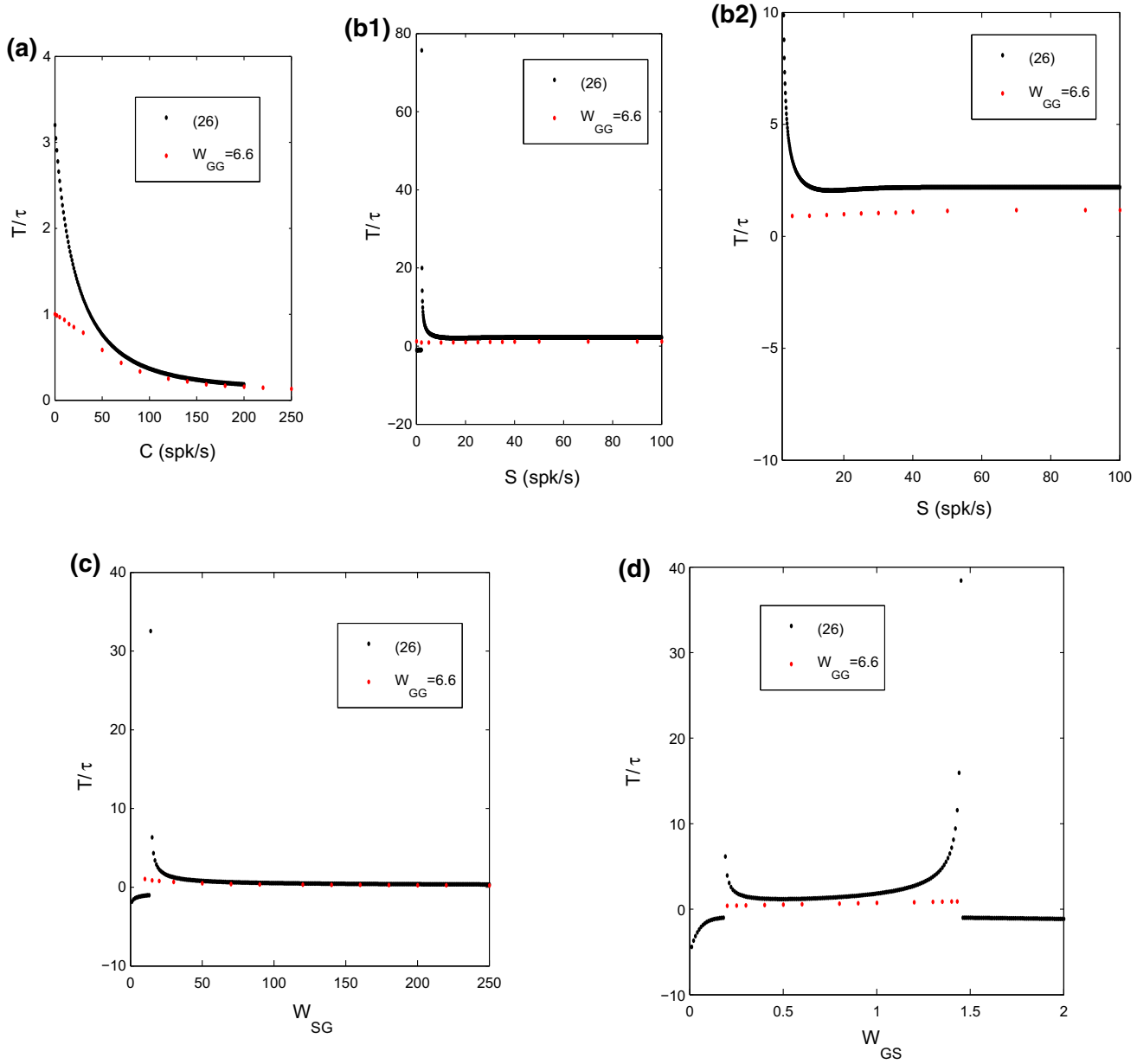

Fig. 11 The effect of the coupling strength W_{GG} on oscillations. Solid lines represent Eq. (26), and red dots denote the simulation results. They show that the effect of W_{GG} is small. In all simulations, we taken $w_{GG} = 6.6$. (Color figure online)

to the typical beta oscillation, other typical frequency ranges also appeared in this model with changes in parameters, such as the typical resting tremor phenomena (4–6 Hz) in Fig. 9d. Therefore, we may infer that the model and method presented in the paper can also be generalized to these situations. The delay is also a key factor in inducing oscillations. As shown in Fig. 5d, oscillation occurred only when the delay was large enough. In addition, the DF decreased with increasing delay. If the delay was too large, oscillation disappeared because the signal was transmitted too slowly. In previous studies, such as in (Holgado et al. 2010), the coupling strength was considered as a whole to explore its effect on oscillations. However, we found that the effects of the W_{SG} and W_{GS} on oscillations are not symmetrical. The minimal value of the W_{SG} required for producing oscillations is obviously larger than that of the W_{GS}, as shown in Figs. 9a and 10a. If W_{GS} exceeds certain values (> 1.5), the oscillation activity will soon disappear. We thought that this behaviour may be because the W_{SG} is the excitatory coupling strength, while the W_{GS} is the inhibitory coupling strength in the network.

In Fig. 1, we highlighted some aspects of this model that should be considered and improved in further research. (1) On the one hand, the model was developed from previous

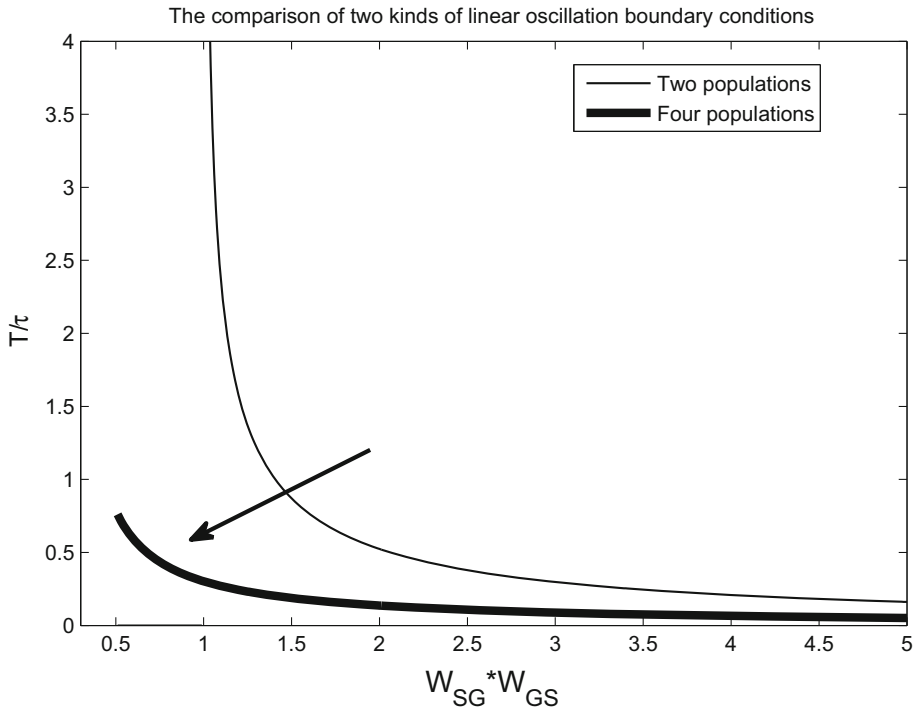

Fig. 12 Comparison of two types of linear oscillation conditions, obtained in (Pavlides et al. 2012) and in this model, respectively. As the number of populations increases, the oscillation curves move to the left, as indicated by the arrow

studies (Holgado et al. 2010; Pavlides et al. 2012) by supposing that the STN and GPe both contain two parts (STN1, STN2,GP1,GP2) because the brain has a large number of neurons; on the other hand, the model is overall simplified, as the coupling strengths on the same type of pathways, and all delays were considered to be equal to facilitate the deduction of a formula for the oscillation conditions. Therefore, if the cortex sends outputs to both the STN1 and STN2, then, in the background of this model, they would become the same population. Similarly, to distinguish between the GP1 and GP2, we suppose that the striatum sends no signals to the GP2 and that intranuclear inhibition is not present between these two parts of the GP. Moreover, in the model, we found that this intranuclear inhibition had little effect on the oscillations and was not considered a critical factor. Of course, the rationality of the model should be further confirmed in spiking models and related experiments. (2) We acknowledge that the cortex exerts great effects on the striatum in the brain. However, in this paper, we mainly emphasized the STN–GPe circuit mechanisms for the generation of beta oscillations, and the cortex and striatum populations were simplified and represented by constant inputs to the STN–GP loop, which did not affect the qualitative study of oscillation conditions in this model. Of course, the cortex–striatum connection should be added in more realistic models in the future. (3) It should be noted that the conductance delay, excitatory synaptic delay and inhibitory synaptic delay are different in the brain, whereas they have been treated as equal in the model because it is difficult to solve equations with two or more different delays. Therefore, future research should consider heterogeneity delays between different connections in spiking models. (4) It is noted that the frequency of beta oscillations is varied with different parameters in this model, however, it is usually more or less fixed and does not vary in experiments. Therefore, this may be a potential problem for similar model studies, which should be further considered in the future. (5) In addition to beta oscillations, some other typical frequency bands also appeared in the model, such as 4–6 Hz oscillations. It is noted that tremor in Parkinson's disease is a phenomenon generated in the cortex-basal ganglia-thalamus loop (Dovzhenok and Rubchinsky 2012), but not all 4 Hz oscillations are tremors. Therefore, whether different frequency oscillations shown in the model are related to Parkinson's disease should be verified in a more realistic model and experiments. We hope that the results obtained in this model can provide a unified framework for future study. (6) It is noted that the stable and oscillatory states are the only two phenomena that appeared in the model, as shown in Fig. 3, and we think that the transition from the stable state to the oscillatory state may be induced by Hopf bifurcation (Marsden and McCracken 2012), which can be further verified in the spiking model in future research. (7) Finally, we compared the linear oscillation condition obtained in this paper with the results in (Holgado et al. 2010). We found that the minimum values of the coupling weights and delays required for producing oscillations decrease as the number of nuclei increases, as shown in Fig. 12. Although the theoretical oscillation conditions are difficult to derive

with further increases in the number of nuclei, we might infer that the trend indicated by the arrow in Fig. 12 is generalized. It should also be noted that the results obtained by the mean field equations are qualitative, and a future, more precise quantitative study should employ the spiking model.

Acknowledgements This research was supported by the National Science Foundation of China (Grant Nos. 11602092); the Natural Science Foundation of Hubei Province (Grant No. 2018CFB628); the China Postdoctoral Science Foundation (Grant No. 2018M632184); the National Undergraduate Training Program for Innovation and Entrepreneurship of Huazhong Agricultural University (Grant Nos. 201710504092, 201810504104) and the Scientific and technological innovation fund for college students (SRF) of Huazhong Agricultural University (Grant No. 2018323).

Appendix

See Table 1.

Table 1 The detailed sources of the parameters employed in the simulations

Parameter	Value	References
T	7 ms	Pavlides et al. (2012), Fujimoto and Kita (1993) and Kita et al. (2005)
τ_s	6 ms	Pavlides et al. (2012), Nakanishi et al. (1987) and Paz et al. (2005)
τ_G	14 ms	Pavlides et al. (2012) and Kita and Kitai (1991)
C	27 spk/s	Pavlides et al. (2012) and Lebedev and Wise (2000)
S	2 spk/s	Pavlides et al. (2012) and Schultz and Romo (1988)
M_S	300 spk/s	Pavlides et al. (2012) and Hallworth et al. (2003)
B_S	17 spk/s	Pavlides et al. (2012) and Hallworth et al. (2003)
M_G	400 spk/s	Pavlides et al. (2012), Kita et al. (2005) and Kita (2007)
B_G	75 spk/s	Pavlides et al. (2012), Kita (2007) and Kita et al. (2004)
w_{GS}	1.12	Holgado et al. (2010) and Pavlides et al. (2012)
w_{GG}	6.6	Holgado et al. (2010) and Pavlides et al. (2012)
w_{SG}	19.0	Holgado et al. (2010) and Pavlides et al. (2012)
w_{CS}	2.42	Holgado et al. (2010) and Pavlides et al. (2012)
w_{XG}	15.1	Holgado et al. (2010) and Pavlides et al. (2012)

References

Ahn S, Zauber SE, Worth RM, Witt T, Rubchinsky LL (2015) Interaction of synchronized dynamics in cortex and basal ganglia in Parkinson's disease. Eur J Neurosci 42(5):2164–2171

Ahn S, Zauber SE, Worth RM, Rubchinsky LL (2016) Synchronized beta-band oscillations in a model of the globus pallidus-subthalamic nucleus network under external input. Front Comput Neurosci 10:134

Alcacer C, Andreoli L, Sebastianutto I, Jakobsson J, Fieblinger T, Cenci MA (2017) Chemogenetic stimulation of striatal projection neurons modulates responses to Parkinson's disease therapy. J Clin Investig 127(2):720–734

Belluscio MA, Escande MV, Keifman E, Riquelme LA, Murer MG, Zold CL (2014) Oscillations in the basal ganglia in Parkinson's disease: role of the striatum. Basal Ganglia 3(4):203–212

Bergman H, Wichmann T, Karmon B, Delong MR (1994) The primate subthalamic nucleus. II. Neuronal activity in the MPTP model of parkinsonism. J Neurophysiol 72(2):507

Brown P, Oliviero A, Mazzone P, Insola A, Tonali P, Di Lazzaro V (2001) Dopamine dependency of oscillations between subthalamic nucleus and pallidum in Parkinson's disease. J Neurosci 21:1033–1038

Camara C, Isasi P, Warwick K, Ruiz V, Aziz T, Stein J, Bakštein E (2015) Resting tremor classification and detection in Parkinson's disease patients. Biomed Signal Proces 16:88–97

Cole SR, van der Meij R, Peterson EJ, De Hemptinne C, Starr PA, Voytek B (2017) Nonsinusoidal beta oscillations reflect cortical pathophysiology in Parkinson's disease. J Neurosci 2017:2208–16

Dasdemir Y, Yildirim E, Yildirim S (2017) Analysis of functional brain connections for positive-negative emotions using phase locking value. Cogn Neurodyn 11(6):487–500

Dayan P, Abbott LF (2001) Theoretical neuroscience. MIT Press, Cambridge

Dovzhenok A, Rubchinsky LL (2012) On the Origin of Tremor in Parkinson's Disease. PLoS ONE 7(7):e41598

Fujimoto K, Kita H (1993) Response characteristics of subthalamic neurons to the stimulation of the sensorimotor cortex in the rat. Brain Res 609(1–2):185

Gillies A, Willshaw D, Li Z (2002) Subthalamic-pallidal interactions are critical in determining normal and abnormal functioning of the basal ganglia. Proc R Soc B Biol Sci 269(1491):545

Hallworth NE, Wilson CJ, Bevan MD (2003) Apamin-sensitive small conductance calcium-activated potassium channels, through their selective coupling to voltage-gated calcium channels, are critical determinants of the precision, pace, and pattern of action potential generation in rat subthalamic nucleus neurons in vitro. J Neurosci 23(20):7525–7542

Holgado AJ, Terry JR, Bogacz R (2010) Conditions for the generation of beta oscillations in the subthalamic nucleus-globus pallidus network. J Neurosci 30(37):12340

Holt AB, Netoff TI (2014) Origins and suppression of oscillations in a computational model of Parkinson's disease. J Comput Neurosci 37(3):505–521

Hu B, Guo Y, Zou X et al (2018) Controlling mechanism of absence seizures by deep brain stimulus applied on subthalamic nucleus. Cogn Neurodyn 12(1):103–119

Humphries MD, Stewart RD, Gurney KN (2006) A physiologically plausible model of action selection and oscillatory activity in the basal ganglia. J Neurosci 26(50):12921

Jankovic J (2008) Parkinson's disease: clinical features and diagnosis. J Neurol Neurosurg Psychiatry 79:368–376

Jiancheng S, Min L, Chusheng H (2017) Cooperative effect of random and time-periodic coupling strength on synchronization

transitions in one-way coupled neural system: mean field approach. Cogn Neurodyn 11(4):1–8
Kim SY, Lim W (2016) Dynamical responses to external stimuli for both cases of excitatory and inhibitory synchronization in a complex neuronal network. Cogn Neurodyn 11(5):1–19
Kim SY, Lim W (2018) Burst synchronization in a scale-free neuronal network with inhibitory spike-timing-dependent plasticity. arXiv:1803.07256
Kita H (2007) Globus pallidus external segment. Prog Brain Res 160(1):111
Kita H, Kitai ST (1991) Intracellular study of rat globus pallidus neurons: membrane properties and responses to neostriatal, subthalamic and nigral stimulation. Brain Res 564(2):296–305
Kita H, Nambu A, Kaneda K, Tachibana Y, Takada M (2004) Role of ionotropic glutamatergic and GABAergic inputs on the firing activity of neurons in the external pallidum in awake monkeys. J Neurophysiol 92(5):3069–84
Kita H, Tachibana Y, Nambu A, Chiken S (2005) Balance of monosynaptic excitatory and disynaptic inhibitory responses of the globus pallidus induced after stimulation of the subthalamic nucleus in the monkey. J Neurosci 25(38):8611
Kumar A, Cardanobile S, Rotter S, Aertsen A (2011) The role of inhibition in generating and controlling Parkinson's disease oscillations in the basal ganglia. Front Syst Neurosci 5:86
Lebedev MA, Wise SP (2000) Oscillations in the premotor cortex: single-unit activity from awake, behaving monkeys. Exp Brain Res 130(2):195
Leblois A, Boraud T, Meissner W, Bergman H, Hansel D (2006) Competition between feedback loops underlies normal and pathological dynamics in the basal ganglia. J Neurosci 26:3567–3583
Levy R, Hutchison WD, Lozano AM, Dostrovsky JO (2000) High-frequency synchronization of neuronal activity in the subthalamic nucleus of parkinsonian patients with limb tremor. J Neurosci 20(20):7766–7775
Little S, Brown P (2014) The functional role of beta oscillations in Parkinson's disease. Parkinsonism Relat Disord 20:S44–S48
Malekmohammadi M, Herron J, Velisar A, Blumenfeld Z, Trager MH, Chizeck HJ, Brontë-Stewart H (2016) Kinematic adaptive deep brain stimulation for resting tremor in Parkinson's disease. Mov Disord 31(3):426–428
Marsden JE, McCracken M (2012) The Hopf bifurcation and its applications. Springer, Berlin
Moustafa AA, Chakravarthy S, Phillips JR, Gupta A, Keri S, Polner B, Frank MJ, Jahanshahi M (2016) Motor symptoms in Parkinson's disease: a unified framework. Neurosci Biobehav Rev 68:727–740
Muralidharan V, Balasubramani PP, Chakravarthy VS, Lewis SJG, Moustafa AA (2013) A computational model of altered gait patterns in parkinson's disease patients negotiating narrow doorways. Front Comput Neurosci 7(7):190
Nakanishi H, Kita H, Kitai ST (1987) Intracellular study of rat substantia nigra pars reticulata neurons in an in vitro slice preparation: electrical membrane properties and response characteristics to subthalamic stimulation. Brain Res 437(1):45–55
Park C, Worth RM, Rubchinsky LL (2011) Neural dynamics in parkinsonian brain: the boundary between synchronized and nonsynchronized dynamics. Phys Rev E 83(4):042901
Pavlides A, Hogan SJ, Bogacz R (2012) Improved conditions for the generation of beta oscillations in the subthalamic nucleus-globus pallidus network. BMC Neurosci 36(2):2229–2239
Pavlides A, Hogan SJ, Bogacz R (2015) Computational models describing possible mechanisms for generation of excessive beta oscillations in Parkinson's disease. PLoS Comput Biol 11(12):e1004609
Paz JT, Deniau JM, Charpier S (2005) Rhythmic bursting in the cortico-subthalamo-pallidal network during spontaneous genetically determined spike and wave discharges. J Neurosci 25(8):2092
Rubin JE, Terman D (2004) High frequency stimulation of the subthalamic nucleus eliminates pathological thalamic rhythmicity in a computational model. J Comput Neurosci 16(3):211
Schiff JL (2013) The Laplace transform: theory and applications. Springer, Berlin
Schultz W, Romo R (1988) Neuronal activity in the monkey striatum during the initiation of movements. Exp Brain Res 71(2):431–6
Shouno O, Tachibana Y, Nambu A, Doya K (2017) Computational model of recurrent subthalamo-pallidal circuit for generation of parkinsonian oscillations. Front Neuroanat 11:21
Surmeier DJ, Graves SM, Shen W (2014) Dopaminergic modulation of striatal networks in health and Parkinson's disease. Curr Opin Neurobiol 29:109–117
Terman D, Rubin JE, Yew AC, Wilson CJ (2002) Activity patterns in a model for the subthalamopallidal network of the basal ganglia. J Neurosci 22:2963–2976
van Albada SJ, Robinson PA (2009) Mean-field modeling of the basal ganglia thalamocortical system. I: firing rates in healthy and parkinsonian states. J Theor Biol 257(4):642–663
van Albada SJ, Gray RT, Drysdale PM, Robinson PA (2009) Meanfield modeling of the basal ganglia-thalamocortical system. II: dynamics of parkinsonian oscillations. J Theor Biol 257(4):664–688
Vogels T, Rajan K, Abbott L (2005) Neural network dynamics. Annu Rev Neurosci 28:357–376
Wang JY, Yang XL, Sun ZK (2018) Suppressing bursting synchronization in a modular neuronal network with synaptic plasticity. Cogn Neurodyn 12(6):625–636
Yi GS, Wang J, Deng B, Wei XL (2017) Complexity of resting-state EEG activity in the patients with early-stage Parkinson's disease. Cogn Neurodyn 11(2):147–160